Environmental Earth Sciences (2024) 83:180
https://doi.org/10.1007/s12665-024-11471-y

ORIGINAL ARTICLE

Hydrological and geochemical properties of bottom ash landfills

Philipp Ingold[1] · Gisela Weibel[1] · Christoph Wanner[1] · Thomas Gimmi[1,2] · Sergey V. Churakov[1,2]

Received: 10 November 2023 / Accepted: 31 January 2024 / Published online: 12 March 2024

Abstract
In Switzerland, municipal solid waste incineration bottom ash is deposited in open landfills, which leads to its interaction with rainwater and thus the formation of a polluted leachate. This study attempts to provide a better understanding of the hydraulic and geochemical properties of bottom ash landfills by combining field and laboratory investigations. The results show that a bottom ash landfill can be described as a generally unsaturated body with several layers of different grain sizes. Three different water domains with variable hydraulic and geochemical properties were identified in the landfill: (1) zones of preferential flow, (2) a reservoir of mobile porewater, and (3) an immobile porewater reservoir. Preferential flow systems account for approximately 5–10 vol.%. The landfill layering is primarily responsible for the formation of various flow systems during heavy rainfall events. The domains and reservoirs provide variable volumetric contribution to the leachate, depending on precipitation rates and duration of dry periods. Sampling of leachate during heavy rainfall events revealed dilution effects for Na (− 59–61% compared to concentrations prior to the event), Ca (− 44–47%), Cl (− 57–77%), and SO_4 (− 35–47%), while *pH* (+7–8%) and concentrations of Al (+368–1416%), Cu (+7–58%), Cr (+29–48%), V (+100–118%), and Zn (+289%) increased significantly. The findings of this study serve as a basis for the development of a hydrogeochemical model of a bottom ash landfill, which allows better prediction of the future evolution of leachate quality.

Keywords Municipal solid waste incineration bottom ash · Landfill aftercare · Preferential flow · Metal mobilization · Bottom ash mineralogy

Introduction

In 2022, Switzerland produced 671 kg of waste per capita, which is above the European average of 600 kg/capita (Eurostat 2023; Federal Office for the Environment 2023). With a recycling rate of 52%, Switzerland was slightly above the average European recycling rate (49.6%). Since the year 2000, the Swiss Waste Ordinance prohibits the disposal of unburnt municipal solid waste (MSW; Swiss Confederation 2023b). Thus, Switzerland is forced to thermal treatment of all combustible waste from industry and household, that cannot be directly recycled.

MSW incineration (MSWI) in Switzerland is conducted in grate furnace systems at temperatures of 800–1000 °C, targeting the destruction of organic waste and pollutants. The thermal destruction of organic matter and pollutants, evaporation of volatile compounds (e.g., heavy metals with low boiling points) and production of dust particles form the initial flue gas that emerges from the combustion chamber. Continuous cooling processes conducted by heat exchangers and flue gas filtering processes lead to collection of ash particles (fly ash, ca. 2% of the initial waste input). The regained energy is used for electricity generation and district heating. Non-combustible waste, partial melts, and unburnt organic matters remain in the incineration chamber, and forms the bottom ash (ca. 20 wt.% of the initial waste input). Wet extraction (i.e., quenching of the bottom ash) represents the dominant method, while dry extraction (i.e., air-cooling of the bottom ash) is barely conducted. Other countries (e.g., Japan) rely on MSWI methods at higher temperatures (> 1200 °C), targeting the complete destruction of organic pollutants (e.g., dioxin, furan) and the vitrification of the incineration residues (Ecke et al. 2000; Tanigaki et al. 2012; Shiota et al. 2017). MSWI represents a heterogeneous treatment process, which is heavily influenced by the waste

✉ Philipp Ingold
philipp.ingold@unibe.ch

[1] Institute of Geological Sciences, University of Bern, Baltzerstrasse 1+3, 3012 Bern, Switzerland

[2] Laboratory for Waste Management, Paul Scherrer Institute, Forschungsstrasse 111, 5232 Villigen, Switzerland

input and local temperature gradients in the furnace during the incineration, which result in MSWI residues of variable chemical and mineralogical composition (Chang et al. 2001; Kitamura et al. 2019; Huber et al. 2020).

In many countries, mineral fractions of bottom ash are used as secondary raw material for road construction and backfilling (van der Sloot et al. 2001; Birgisdóttir et al. 2006; Dabo et al. 2009; Spreadbury et al. 2021). Due to strict threshold values defined in the Swiss Waste Ordinance, recycling of bottom ash as a secondary raw material is not feasible in Switzerland (Swiss Confederation 2023b). Thus, the MSWI residues must be deposited in landfills. The Swiss Waste Ordinance defines five types of landfills (A–E) in which waste is deposited, depending on its degree of pollution. Landfills of Type D are considered as disposal locations for MSWI residues. The quality criteria for the disposal of bottom ash are TOC < 2 wt.% and non-ferrous metal content < 1 wt.% (Swiss Confederation 2023b). The TOC content is mainly controlled by optimizing the incineration process, while the bottom ash is mechanically processed to reduce the metal content (Mehr et al. 2021). The treated bottom ash is usually placed on the landfill temporarily (up to several weeks) before being deposited in layers of ca. 50 cm and compacted with a roller.

Since bottom ash landfills are exposed to the atmosphere at the surface, infiltration of rainwater into the deposited material occurs. The contact of water with the reactive incineration residues results in the formation of a contaminated leachate. To prevent drainage of such leachates into the soil and groundwater systems, the landfill body is sealed at the bottom with base liner systems. Naturally occurring surface water (e.g., slope water) is discharged in a separate discharge system, while contaminated leachate is discharged into the sewage system. The Swiss Water Protection Act defines threshold values that a landfill leachate must fulfill (Swiss Confederation 2023a). Switzerland's concept of the aftercare of landfills defines an aftercare phase of a minimum of 15 years, and a maximum of 50 years (Swiss Confederation 2023b). The contaminated leachate should not cause any hazardous effects on the environment after completion of the aftercare phase. Therefore, it should be possible to discharge the leachate into a nearby surface water system. As the future leachate development is associated with major uncertainties, a hydrogeochemical model can help the assessment of long-term leachate quality and an improved bottom ash landfill management.

The reactivity of bottom ash is given due to its thermodynamic disequilibrium with atmospheric conditions. The chemical and mineralogical characterization of incineration residues and their alteration reactions have been studied in detail in the last decades (e.g., Eighmy et al. 1994; Meima and Comans 1997; Johnson et al. 1998, 1999; Chimenos et al. 2000; Shimaoka et al. 2007; Saffarzadeh et al. 2011; Alam et al. 2019). However, more detailed insights on the geochemical and hydraulic properties of deposited bottom ash are necessary to determine future leaching behavior (Eighmy et al. 1994; Eusden et al. 1999; Piantone et al. 2004; Bayuseno and Schmahl 2010). Furthermore, environmental conditions (i.e., water balance, physical properties of residues, landfill shape, and filling practice) are mostly not considered in leaching scenarios. These parameters have a significant impact and controlling factor on leaching behavior of bottom ash and thus leachate contamination (Johnson et al. 2001; Sabbas et al. 2003).

The aim of this study is to gain a better understanding of the coupling between hydraulic and geochemical processes taking place in bottom ash landfills. Hydraulic and mineralogical properties of deposited bottom ash have been identified at four typical bottom ash landfills in Switzerland. The field and laboratory tests were combined with extensive leachate sampling campaigns. The results of this study enable a better insight on the poorly understood landfill system and serve as a basis for the development of a hydraulic and geochemical model of a bottom ash landfill. This model will be developed in a follow-up study and will provide a better prediction of future leachate quality trends.

Materials and methods

Investigated landfills

Four different bottom ash landfills, containing seven type D compartments with various age of deposits, material type and activity were selected for this study (Supplementary Table 1). All sites represent open systems (i.e., no surface cover equipped on any of the compartments). There are landfills with pure wet extracted bottom ash, with dry extracted bottom ash or also with mixtures. Landfill I contains only wet extracted bottom ash, while the investigated landfill IV compartment represents a dry extracted bottom ash type. At landfill II and III, a mixture of wet and dry extracted bottom ash is actively deposited. The older, inactive compartments (II1, III1, III2) contain wet extracted bottom ash only. Meteorological data (e.g., precipitation, humidity, and temperature) are measured directly on the landfill sites. Discharge, electrical conductivity, and temperature are continuously monitored in the landfill drainage systems.

Sampling methods

Samples of bottom ash prior to disposal were collected for solid analysis (samples I—IV). On each site I—III, a sample size of 20 kg of fresh treated bottom ash (i.e., after metal separation) was collected each day over a period of 10 days, while the dry extracted bottom ash was collected

directly after incineration and treatment at the MSWI plant, following the same procedure. Representative sampling and splitting were maintained according to the Swiss Guidelines (Federal Office for the Environment 2022).

Leachate samples of the various landfill compartments (Supplementary Table 1) were collected directly from the drainage pipe system at regular biweekly intervals over a period of several months (i.e., repetitive sampling of leachate and regardless of external circumstances). The actual outflow of each pipe per compartment was sampled over the duration of one minute and a composite sample was prepared which is representative of the water conducted per pipe. An automatized sampling system (Liquiport CSP 44, Endress + Hauser) was used for event-triggered (i.e., dynamic) sampling of leachate during two heavy rain events on landfill I. On event 1, samples were collected over a 24-h period at a 60-min time interval. For event 2, samples were collected over a 36-h period at a 90-min time interval. On-site monitoring by the landfill operator was used for automatization of the sampling sequence. Decrease of electrical conductivity (*EC*) under a certain value was used as a starting trigger. If a sustained duration of the event was verified in the monitoring data, the sampling system was manually restarted after collecting the samples, thus continuing the sampling sequence.

Field tests

For visualization of water flow paths passing through the landfill, a tracer experiment using brilliant blue FCF (Instant Sunshine™) was performed on landfill IV. In this experiment, 40 L of a dyed solution ($c_{Brilliant\ Blue} = 5$ g/L) was homogeneously applied on a pre-wetted (V = 100 L) surface (A = 1.40 m^2) over 2 h. This corresponds to an infiltration rate of 14.3 mm/h. Both the pre-wetting and the dye tracer application were stopped as soon as generation of surface runoff was observed. This ensures a complete infiltration into the landfill. After 16 h, a trench was opened to a depth of 3 m focusing on the repetitive disposal sequences. In order to visually document the percolation of the tracer solution, multiple vertical profiles within the dyed area were exposed (i.e., removing deposited material in multiple slices with an excavator). In addition, water content samples were taken along the profiles as a function of depth.

Soil extraction cylinders were hammered into the deposited bottom ash used for determining site-specific physical parameters. A workflow of weighting, saturating for 16–24 h and drying allowed determination of initial (i.e., natural) water content, saturated water content, dry packing density and porosity. Seasonality was considered by sampling under variable weather conditions along the year between June 2021 and August 2022. Such samples were mainly taken from the surface of the landfill, but also on the vertical profile section excavated during the tracer experiment in landfill IV.

Leaching experiments

Eluate tests were performed to evaluate the leaching behavior of bottom ash under standardized conditions, following the instructions of the Swiss waste guidelines (Test 2; Federal Office for the Environment 2022). 170 g of fresh sampled bottom ash of landfill I was weighted in a glass bottle and stirred with water (L/S = 10 L/kg) by an overhead shaker (1 r/min) over 24 h. *EC* and *pH* were determined directly in the glass bottle and leachate samples were taken and filtered for further analysis. To reduce material effects (i.e., heterogeneity of the bottom ash sample) and to validate the measured concentration values, the experiments were conducted in duplicate.

Solid-phase analysis

Compaction tests (i.e., proctor experiments) and determination of the hydraulic conductivity (K_{sat}) were conducted, following the instructions described in EN 13286-2 (proctor experiments) and EN 17892-11 (determination of K-value). The bottom ash sample was dried, rewetted and mixed with a previously determined amount of water, and then stored for 16 h before performing the experiment. For determination of the grain size distribution, a sampled bottom ash batch was dried and then sieved, following the instructions of EN 17892-4.

For mineralogical investigation, a sampled batch was dried at 40 °C and milled to grain sizes < 0.1 mm. The sample was mixed with corundum as internal standard using a McCrone XRD-mill (Retsch) and measured with X-ray powder diffraction (XRPD; Empyrean, Malvern Panalytical) using Cu-K-Alpha wavelength (40 kV, 30 A). The quantification of mineral phases was achieved by Rietveld refinement using the software Topas (Bruker).

Solution-phase analysis

Concentrations of Al, B, Ba, Ca, Cd, Co, Cr, Cu, Fe, K, Mg, Mn, Mo, Na, Ni, Pb, Sb, Si, Ti, V and Zn were determined using an ICP-System (ICP-OES ICap 7600, Thermo Fisher Analytics and ICP-MS Nexlon 2000, Perkin Elmer) with a detection limit of 0.01 mg/L. Filtered samples (0.45 µm filter) were treated with IC preparation cartridges for exchanging cations with H^+ (IC-H, Metrohm) and then analyzed using IC (850 Professional, Metrohm) for determining concentrations of F^-, Cl^-, Br^-, NO_3^-, PO_4^{3-} and SO_4^{2-} with detection limits of 2 mg/L for F^-, Cl^-, Br^-, NO_3^-, and SO_4^{2-}, and 5 mg/L for PO_4^{3-}. Dissolved carbon

concentrations (DOC, DIC, and DC) were determined using Multi N/C 2100S (Analytik Jena) with a detection limit of 5 mg/L.

PHREEQC modeling

Based on the mineralogical composition, leaching experiment conditions were simulated and leachate composition at equilibrium conditions were calculated with the help of the USGS open-source code PHREEQC (Parkhurst & Appelo 2013). As the leaching behavior is subject to many uncertainties, tracing of mobilization and leaching effects by this model is limited to the identified mineral phases. To reduce the number of phases, the system was simplified by using one phase as representative for an entire mineral group (i.e., quartz for SiO_2-phases, diopside for pyroxenes, magnetite for Fe-oxides, goethite for Fe-alteration phases, and anorthite for feldspars). Detailed characterization of mineralogical and chemical composition of Swiss bottom ashes can be found in previous studies (e.g., Eggimann 2008; Glauser 2021). For the calculations, the Wateq4f database was used and equilibrium constants (Log K values) of lime and ettringite were added from the llnl-database (Lawrence Livermore National Laboratory). Akermanite ($Ca_2MgSi_2O_7$) and gehlenite ($Ca_2Al_2SiO_7$) were not implemented in the simulation, as their solubility is low under given pH conditions (Engström et al. 2013). An initial interaction of the water with the atmosphere was assumed, allowing CO_2 uptake, while for all following reactions with the bottom ash mineral phases, a closed system without any further contact to the atmosphere was assumed.

Results

Physical and mineralogical properties of bottom ash

All bottom ashes showed a generally well-graded grain size distribution with a d_{50} value of 4 mm (min. 2, max. 7 mm). Depending on treatment and metal recovery strategy, the maximum grain size ranged between 15 and 35 mm, whereby large grains were mostly identified as metallic residuals (Table 1).

The water content of deposited bottom ash is mainly controlled by weather conditions and showed seasonal variation with a mean value of 17.2 wt.% relative to the dry mass. The saturated water content of all bottom ashes showed a mean of 34.3 wt.% relative to the dry mass. Dry density of field samples was on average 1.50 Mg/m^3 with a mean porosity of 50 vol.% (Table 1).

Higher compaction densities compared to the field tests were achieved with the proctor experiments with dry density ranging from 1.47 Mg/m^3 up to 1.70 Mg/m^3 with variable water contents. Highest compaction was reached by adding 11.4 wt.% (relative to the dry mass) to the bottom ash material. The laboratory tests showed mean porosity values of 32 vol.% and K_{sat} values of 7.3 10^{-7} m/s to 2.6 10^{-4} m/s (Table 1).

Table 1 Geotechnical and hydraulic properties of the investigated fresh bottom ashes, including maximum and mean grain size (d_{max} and d_{50}, respectively, $N=4$), initial and saturated water content (w_{init} and w_{sat}, respectively, $N=32$), experimental water content used during proctor experiments (w_{exp}), mean compaction densities (ρ_{mean}) and porosity (φ_{mean}) determined on the landfill ($N=32$) and in the laboratory ($N=37$), and saturated conductivity (K_{sat}, $N=8$)

	Unit	Mean	SD	Min	Max
d_{max}	mm	25	10	15	35
d_{50}	mm	4	2.65	2	7
Gravel (2–63 mm)	wt.%	62.3	15.7	48.3	79.3
Sand (0.063–2 mm)	wt.%	30.8	12.1	18.0	42.0
Silt (0.002–0.063 mm)	wt.%	6.9	3.7	2.7	9.7
Clay (< 0.002 mm)	wt.%	0.0	0.0	0.0	0.0
w_{init} (field)	wt.%	18.2	3.3	9.3	22.7
w_{sat} (field)	wt.%	34.3	3.6	24.0	40.7
ρ_{mean} (field)	Mg/m^3	1.50	0.08	1.36	1.75
φ_{mean} (field)	vol.%	51.4	3.7	42.0	62.9
w_{exp} (lab)	wt.%	11.5	-	3.1	19.3
ρ_{mean} (lab)	Mg/m^3	1.60	0.07	1.47	1.74
φ_{mean} (lab)	vol.%	32.1	2.5	28.3	34.5
K_{sat}	m/s	$3.0 \cdot 10^{-5}$	$8.6 \cdot 10^{-5}$	$7.3 \cdot 10^{-7}$	$2.6 \cdot 10^{-4}$

Mineralogical composition of the studied bottom ashes is reported in the appendix (Supplementary Table 2). Samples I–III showed high fractions of amorphous phases (61–75 wt.%). Minerals of the melilite group (i.e., akermanite and gehlenite) represented the main mineral phase with 9.0–9.7 wt.%. The SiO_2-phases (i.e., quartz and cristobalite) together accounted for 6.0–8.2 wt.%. Augite and diopside were selected as representatives for pyroxenes, which showed together weight fractions ranging between 4.0 and 4.8 wt.%. Fe-oxides (i.e., magnetite, wuestite and magnesioferrite, up to 3.9 wt.%), carbonates (i.e., calcite, siderite, magnesite, and vaterite, up to 4.8 wt.%) and feldspars (i.e., anorthite, albite, and orthoclase, up to 1.7 wt.%) were present in smaller weight fractions. Alteration products of iron bearing phases (i.e., goethite and hematite), as well as phases formed by water uptake of anhydrite (i.e., bassanite), were identified in larger fractions in wet extracted bottom ash samples (i.e., bottom ash of landfill I) and mixed samples which were dominated by wet extracted bottom ash (i.e., bottom ash of landfill II). Free metals (i.e., aluminum, copper, and iron) were detected in all samples but never showed values above 1 wt.%.

Dry extracted bottom ash sample (sample IV) allowed identification of the mineralogy of bottom ash directly after incineration (i.e., no water applied to the sample). Comparison of this sample with the samples I–III allowed identification of early mineral reactions, which were triggered by contact with water (during quenching after incineration for generation of wet extracted bottom ash or during wetting of dry extracted bottom ash for transportation to the landfill). Sample IV showed a lower amount of amorphous fraction (50.3 wt.%). SiO_2-phases were dominant in the sample with a weight fraction of 15.4 wt.%, followed by carbonates (8.4 wt.%) and melilite (7.7 wt.%). Other silicates, such as wollastonite and perovskite were present in smaller weight fractions with various amounts. Compared to the landfill bottom ashes (samples I–III), clinker phases such as alite and belite were present in higher proportions. Furthermore, lime and portlandite were detected in the dry extracted bottom ash sample in small fractions (below 1 wt.%), while no landfill sample showed detectable weight fractions of these phases. Furthermore, salts (halite and sylvite, 1.2 wt.%) and anhydrite (1.9 wt.%) were found in quantitative weight fractions in the dry extracted bottom ash sample compared to the in the landfill bottom ash samples (I–III) (Supplementary Table 2).

Visualization of landfill structure

A vertical cross-section sketch of the upper 2.5 m of a bottom ash landfill is shown in Fig. 1. It illustrates the internal structure of the bottom ash landfill and the typical patterns observed after dye infiltration (Supplementary Fig. 1). In general, the landfill showed horizontally orientated layering due to the compaction with the roller. Grain destruction led to generation of finer grained layers, which represented top layers of a disposal sequence (Fig. 1, Supplementary Fig. 1). Horizontal textures were observed in the finer grained layers, which typically showed a thickness of 5–15 cm (Fig. 1, Supplementary Fig. 1). The finer grained sections tend to form hard, compact structures. The effect of compaction decreased with increasing depth, resulting in a gradual transformation to coarse-grained bottom ash layers. Upper lying, younger disposal sequences were separated with a sharp border. These underlying layers with grainsizes > 10 mm were not affected by compaction and maintained the internal structure initially formed during disposal. A reduced stability of the coarse-grained sections was noticed as material detached from these sections during the excavation process. With a thickness of 20–35 cm, the coarse-grained sequence showed a thickness more than twice the fine-grained sequence (Fig. 1, Supplementary Fig. 1). The larger grains formed a skeletal structure in the coarse-grained layers, with finer material filling up empty space between large grains and can easily be excavated due to decomposition of the skeletal structure.

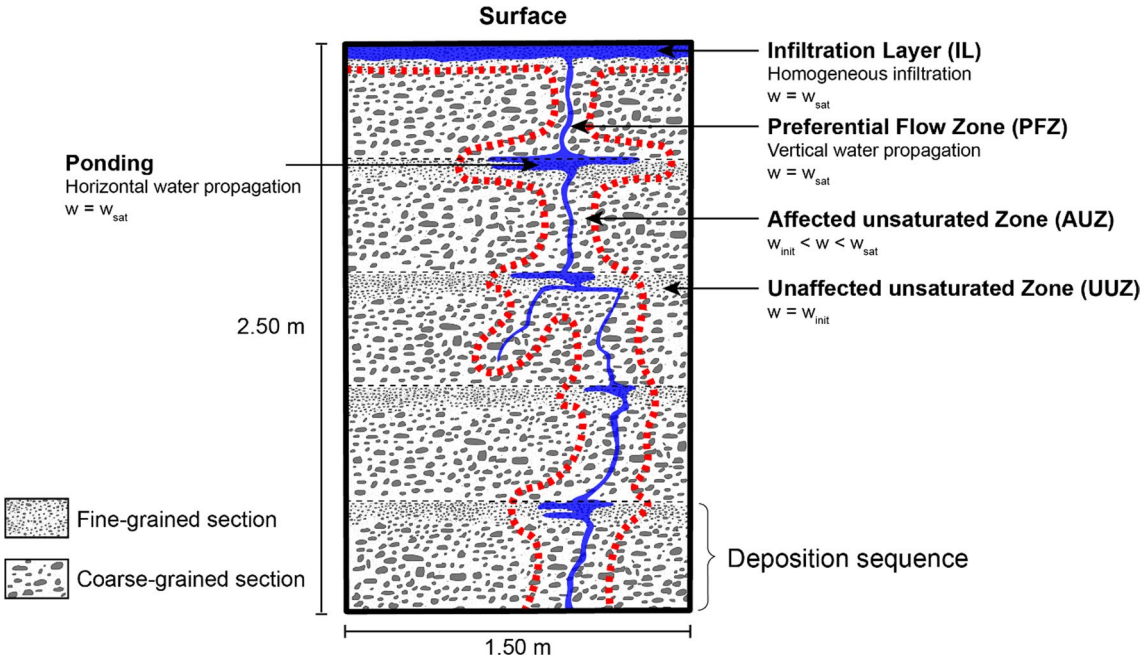

Fig. 1 Graphical illustration of the structure and dye solution propagation during the tracer experiment, showing the fine-/coarse-grained layering and the various water flow zones, which are related to heterogeneous water flow

Leachate composition during regular sampling

The regular sampling of the various leachates represented background concentration values that can be expected from bottom ash landfills (Table 2). With *pH* values ranging between 7.19 and 9.26, all leachate samples showed neutral to slightly alkaline *pH* conditions. *EC*, which acts as a proxy for solute content, showed also a variation across the different compartments, with values between 14.9 and 28.4 mS/cm. Consequently, main ions (i.e., Na, K, Ca, Mg, Cl, SO_4, HCO_3, and NO_3) showed large variations of concentrations as well. Figure 2 shows the relative concentration of major cations and anions (in % meq/L) of the investigated compartments (I, II1, II2, III1, III2, III3, and IV). Detailed concentration values of each compartment are listed in the appendix (Supplementary Table 3). Na and K, and often also Ca, represented the main cations in all leachate samples. The anionic composition varied with Cl and SO_4 being present in various proportions to each other. During the regular sampling, it was noted that *pH* and *EC* increased with decreasing discharge during dry conditions (i.e., low precipitation season).

Potentially toxic elements (i.e., heavy metals) and other components with defined threshold values (e.g., DOC; Swiss Confederation 2023a) only accounted for minor fractions of solute content. However, these elements are of interest in the context of limit assessment for discharge into sewage and later near surface systems. *pH*, Cu, Mo, and DOC were identified as critical parameters that potentially exceed the threshold values (Table 2). For instance, leachate samples of landfill IV showed elevated concentrations for all these parameters (Supplementary Table 3). Other trace metals such as Al, Cr, Fe, Pb, Sb, V and Zn showed concentrations below 1 mg/L (Al and Fe), 0.5 mg/L (Zn) and 0.2 mg/L (Cr, Pb, Sb and V), respectively. In case of Cr, Pb and Zn, all current restrictions were fulfilled (Table 2).

Leachate composition during heavy precipitation events

Figure 3 shows plots of *Q*, *pH*, *EC*, and selected element concentrations of leachate samples, which were taken during heavy precipitation events in December 2021 (event 1, 25.2 mm/23 h) and September 2022 (event 2, 55 mm/38 h) on landfill I. Table 4 shows the comparison of samples collected during both events at maximum discharge and concentrations from continuous monitoring at landfill I. The complete analyses are listed in the appendix (Supplementary Table 5).

Table 2 Mean, standard deviation (SD), minimum and maximum concentration values of selected parameters, measured in the leachate samples of all landfills (I–IV). Threshold values defined by the Swiss Water Protection Act (Swiss Confederation 2023a) are added as additional columns

	Unit	All landfills	Threshold values				
		Mean	SD	Min	Max	Sewage system	Surface water
Q	L/min	5.73	5.10	0.60	24.0	–	–
pH	-	7.96	0.37	7.19	9.26	6.5–9.0	6.5–9.0
EC	mS/cm	21.7	6.73	5.58	37.5	–	–
Na	mg/L	4505	1721	913	9239	–	–
K	mg/L	972	335	196	1712	–	–
Ca	mg/L	328	150	88.5	675	–	–
Mg	mg/L	26.8	12.9	3.33	54.1	–	–
Cl	mg/L	5421	1930	817	9522	–	–
SO_4	mg/L	3740	1806	1190	8529	–	–
HCO_3	mg/L	287	261	45.4	1402	–	–
NO_3	mg/L	252	210	1.96	678	–	–
Al	mg/L	3.88E-01	6.90E-01	1.70E-02	3.20	–	–
B	mg/L	6.03	4.61E+00	4.17E-01	1.51E+01	–	–
Cr	mg/L	7.77E-02	9.25E-02	1.30E-02	5.62E-01	2	2 (0.1 Cr^{VI})
Cu	mg/L	8.53E-01	1.37	3.00E-02	5.90	1	0.5
Fe	mg/L	3.69E-01	7.00E-01	1.10E-02	4.03	–	–
Mo	mg/L	1.58	1.13	6.10E-02	3.91	1	–
Ni	mg/L	5.56E-02	4.39E-02	1.10E-02	1.92E-01	2	2
Pb	mg/L	3.46E-02	3.46E-02	1.10E-02	1.36E-01	0.5	0.5
Sb	mg/L	6.98E-02	4.84E-02	1.10E-02	1.66E-01	–	–
V	mg/L	3.15E-02	2.27E-02	1.00E-02	1.00E-01	–	–
Zn	mg/L	1.52E-01	2.20E-01	1.00E-02	8.89E-01	2	2
DOC	mg/L	39.9	39.0	5.64	119	–	10

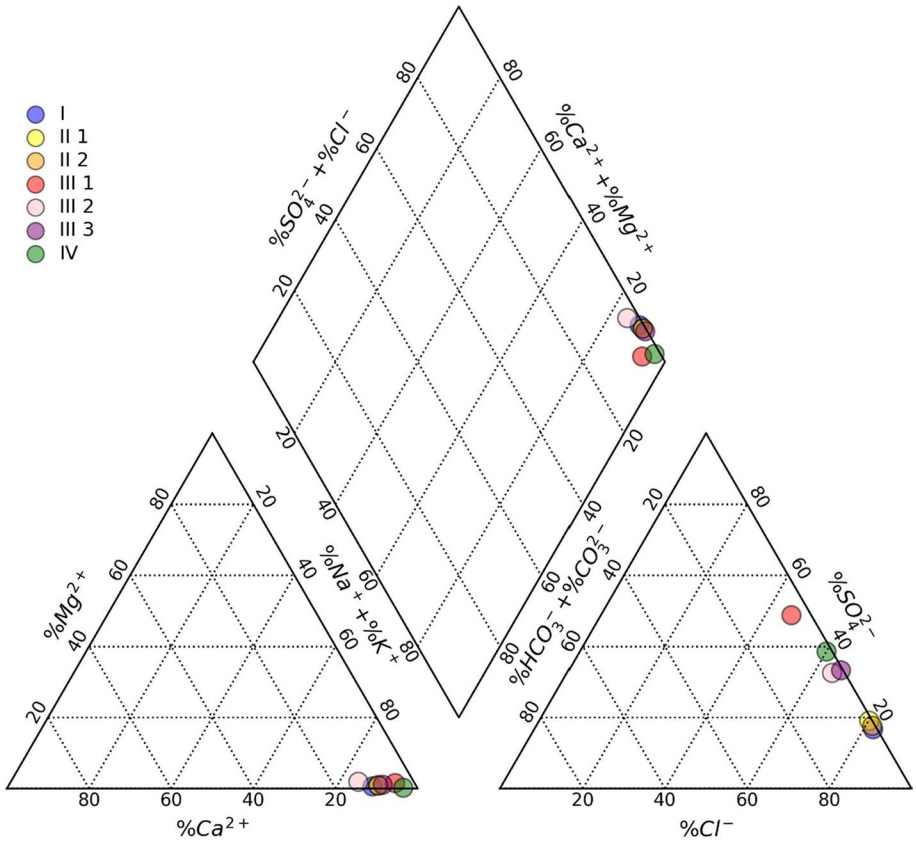

Fig. 2 Piper plot of the average leachate composition of the various compartments (in % meq/L). For the detailed concentration values and compartment properties, see supplementary tables (Supplementary Table 1 and 3) in the appendix

During both events ([1] for event 1, [2] for event 2), *pH* of the leachate showed a relative increase (initial *pH*: 7.39 [1]/8.12 [2], max. *pH*: 7.90 [1]/8.76 [2]) with increasing discharge (initial *Q*: 13.4 L/min [1]/14.9 L/min [2], max. *Q*: 82.5 L/min [1]/824 L/min [2]). The *EC* value decreased relatively strongly in both sampling series (initial *EC*: 16.7 mS/cm [1]/20.4 mS/cm [2], min. *EC*: 8.92 mS/cm [1]/6.35 mS/cm [2]), which is also visible in concentration values of main ions such as Na (initial c_{Na}: 3487 mg/L [1]/3711 mg/L [2], min. c_{Na}: 1517 mg/L [1]/973 mg/L [2]) and Cl (initial c_{Cl}: 5799 mg/L [1]/5926 mg/L [2], min. c_{Cl}: 2466 mg/L [1]/1391 mg/L [2]). Mg showed different trends with a slight increasing trend during event 1 (initial c_{Mg}: 19.0 mg/L, max. c_{Mg}: 23.1 mg/L), while a decrease was observed during event 2 (initial c_{Mg}: 14.7 mg/L, min. c_{Mg}: 8.33 mg/L). Decreasing concentrations trends similar to those of the main ions are observed for Mo (initial c_{Mo}: 0.997 mg/L [1]/1.02 mg/L [2], min. c_{Mo}: 0.525 mg/L [1]/0.283 mg/L [2]) and B (initial c_B: 1.32 mg/L [1]/1.61 mg/L [2], min. c_B: 0.769 mg/L [1]/0.840 mg/L [2]). DOC on the other hand showed no significant effect and slight fluctuations during both events. For Al (initial c_{Al}: 0.053 mg/L [1]/0.159 mg/L [2], max. c_{Al}: 0.248 mg/L [1]/2.41 mg/L [2]), Fe (initial c_{Fe}: < 0.01 mg/L [1]/0.043 mg/L [2], max. c_{Fe}: 0.133 mg/L [1]/0.811 mg/L [2]), and V (initial c_V: 0.014 mg/L [1]/0.017 mg/L [2], max. c_V: 0.019 mg/L [1]/0.037 mg/L [2]), increasing concentrations were noted during both events. In the case of Fe during event 1, concentration values above detection limit were measured specifically during the discharge increase, while no Fe was detectable prior to the precipitation events. During event 1, Cu (initial c_{Cu}: 0.027 mg/L, max. c_{Cu}: 0.029 mg/L) and Cr (initial c_{Cr}: 0.014 mg/L, max. c_{Cr}: 0.018 mg/L) concentrations showed stable conditions, while Zn (initial c_{Zn}: 0.017 mg/L, min. c_{Zn}: < 0.01 mg/L) and Sb (initial c_{Sb}: 0.051 mg/L, min. c_{Sb}: 0.035 mg/L) concentrations decreased, with Zn decreasing below the detection limit (Fig. 3). On the other hand, during event 2, concentration values of these ions (initial c_{Zn}: 0.054 mg/L, max. c_{Zn}: 0.21 mg/L; initial c_{Sb}: 0.065 mg/L, min. c_{Sb}: 0.079 mg/L) showed a clear increase with increasing discharge (Fig. 3). Pb, which was normally below detection limit, was measured during the heavy precipitation event in September 2022 (max. c_{Pb} 0.041 mg/L).

Simulation of leachate generation in the landfill body

The samples leachates at each landfill represent results of individual interaction of water and bottom ash and are strongly controlled by environmental conditions. To gain a deeper insight into the interaction times (i.e., residence time, which varies as a function of water flow velocity)

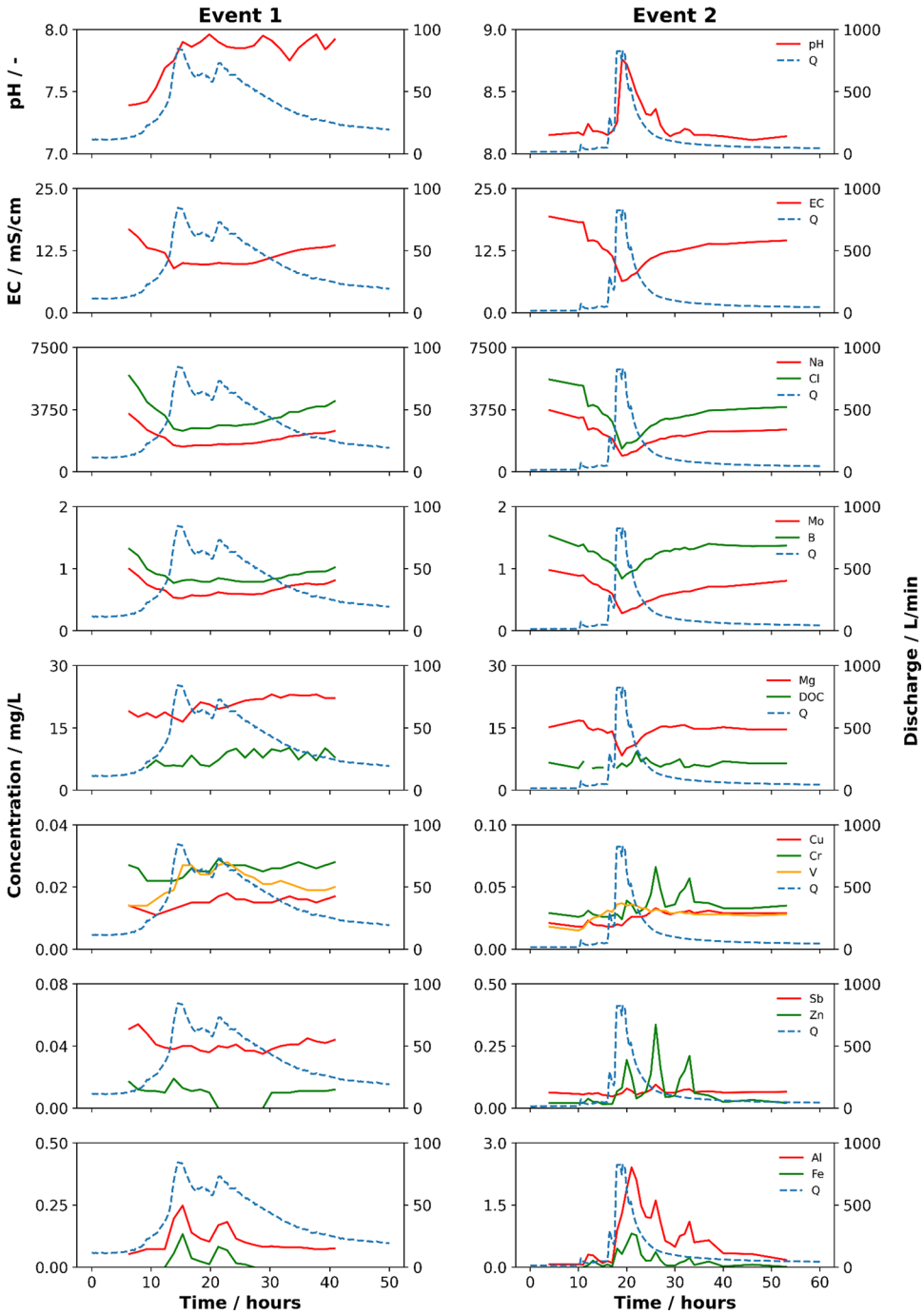

Fig. 3 Discharge *Q*, *pH*, and concentration trends of selected elements during heavy rain events in December 2021 (event 1) and September 2022 (event 2) as a function of time. The Y-axes ranges for discharge, *pH* and some element concentrations vary for the two events due to different measurement ranges

between bottom ash and water, leaching experiments and speciation modeling were combined. The eluate tests simulate approximate equilibrium conditions (i.e., long residence time) between water and bottom ash and the results were verified with thermodynamic speciation calculations. Table 4 shows measured values of *EC* and *pH* and selected concentration values of the leaching experiments. Overall, the samples showed similar *pH*, *EC*, and concentration values. In comparison to the average leachate samples of landfill I (Table 3), *pH* of the leaching solutions showed high values, while *EC* is significantly lower. Similar to landfill leachates, Na, K, and Ca were identified as dominant cations, while Cl and SO_4 represented the main anions in the solutions. In context of trace elements and DOC, measured concentrations generally showed similar values in the experimental solutions compared to the landfill leachates. Al and DOC were identified as the only exception, showing higher concentrations with values around 17.0 mg/L and 16.5 mg/L, respectively.

Table 3 Chemical composition and selected geochemical parameters of leachate of Landfill I from the regular sampling in comparison to samples of the heavy precipitation events 1 (December 2021) and 2 (September 2022), taken at maximum leachate discharge (*Q*)

	Unit	Landfill I				Event 1	Event 2
		Mean	SD	Min	Max		
Q	L/min	12.58	2.19	9.50	15.21	82.5	824
pH	-	7.85	0.14	7.60	8.09	7.90	8.76
EC	mS/cm	22.40	2.45	19.39	26.60	10.00	6.35
Na	mg/L	4006	394	3496	4498	1517	1446
K	mg/L	1198	85.9	1086	1325	510	296
Ca	mg/L	494	48.8	410	576	231	280
Mg	mg/L	19.4	2.01	15.0	21.5	16.5	10.8
Cl	mg/L	6804	746	5771	7683	2466	1391
SO_4	mg/L	1910	203	1699	2241	938	999
HCO_3	mg/L	149	22.8	112	193	182	97.3
NO_3	mg/L	150	26.1	99.1	181	71.3	45.6
Al	mg/L	1.39E-01	1.74E-01	5.10E-02	5.63E-01	2.48E-01	1.29
B	mg/L	1.64	2.30E-01	1.43	2.15	8.10E-01	8.40E-01
Cr	mg/L	1.89E-02	3.18E-03	1.50E-02	2.40E-02	1.40E-02	1.90E-02
Cu	mg/L	3.66E-02	8.19E-03	3.00E-02	5.60E-02	2.30E-02	2.40E-02
Fe	mg/L	2.01E-01	2.75E-01	1.70E-02	5.17E-01	1.33E-01	3.19E-01
Mo	mg/L	1.16	1.17E-01	1.01	1.36	5.25E-01	2.83E-01
Ni	mg/L	< 0.01				1.00E-02	< 0.01
Pb	mg/L				0.02*	< 0.01	1.90E-02
Sb	mg/L	6.06E-02	8.25E-03	5.40E-02	7.70E-02	4.00E-02	6.00E-02
V	mg/L	1.68E-02	3.45E-03	1.40E-02	2.30E-02	2.70E-02	3.70E-02
Zn	mg/L	4.63E-02	4.30E-02	1.80E-02	1.43E-01	1.30E-02	8.10E-02
DOC	mg/L	10.4	7.82	5.64	28.2	5.76	6.46

*Single value, while other samples show concentrations below detection limit

The speciation modeling of the eluate tests with PHREEQC resulted in an aqueous solution, of which the *pH* and concentration values of Na, Ca, Mg, Cl, SO_4, Al, and Fe are shown in Table 4. Halite (NaCl) and anhydrite ($CaSO_4$) were assumed as the main source of Na, Ca, Cl and SO_4 in the aqueous solutions of both the landfill leachates and the experiments. Since both phases were not quantitatively detected with the XRPD (Supplementary Table 2), they were added to adjust the Na and Ca concentration of the model to the measured concentrations. Saturation indices (*SI*) and their residual amount present after the interaction with the liquid are shown in the appendix (Supplementary Table 4).

The pH conditions in the modeled solution showed lower values compared to the experimental solutions. While Na and Ca concentrations of the models matched the measured values, Cl was slightly higher in the modeled solution, while SO_4 showed lower concentrations with respect to the experimental solutions. Al concentrations in the experimental solutions were up to 12 times higher than the thermodynamic model predictions for the given conditions.

During the interaction, the thermodynamic modeling indicated that anhydrite and halite were completely dissolved. Anorthite, calcite, diopside, and magnetite were partly dissolved (Supplementary Table 4). Gibbsite, goethite, and quartz were identified as net precipitating phases, as indicated by a mass gain (positive delta values). Other secondary phases such as ettringite and gypsum showed negative *SI* values, which indicated that these phases remained undersaturated at the present conditions and consequently did not precipitate.

Discussion

Structural heterogeneities and water flow in a landfill

The observations made after the tracer experiment agree well with the data reported in previous studies (Johnson et al. 1998; Sabbas et al. 2003). A bottom ash landfill can be described as an unsaturated body (w_{init} ~ 18.2 wt.%) with several layers of different grain sizes, similar to natural soils.

During dry conditions (i.e., low precipitation season), drying out of the landfill occurs through evaporation and drainage with discharge volume decreasing as a function of time, caused by a reduction of mobilizable fluid in the pore-water systems and a major decrease of the hydraulic conductivity. The variable pore size distributions of the mobile

Table 4 Leachate composition of the eluate tests with bottom ash of landfill I (L/S = 10 L/kg) and composition of the modeled solution

	Unit	Eluate I.1	Eluate I.2	Modeled solution
pH	-	11.44	11.4	10.2
EC	mS/cm	2.19	2.19	-
Na	mg/L	264	260	260
K	mg/L	106	104	-
Ca	mg/L	61.8	62.9	62.7
Mg	mg/L	0.21	0.24	0
Cl	mg/L	387	363	402
SO_4	mg/L	186	199	124
HCO_3	mg/L	14.3	27.2	1.12
NO_3	mg/L	0.3	0.22	–
Al	mg/L	16.9	17.4	1.38
B	mg/L	< 0.01	< 0.01	–
Cr	mg/L	0.03	0.03	–
Cu	mg/L	0.03	0.03	–
Fe	mg/L	< 0.01	< 0.01	0
Mo	mg/L	0.13	0.12	-
Ni	mg/L	< 0.01	< 0.01	–
Pb	mg/L	< 0.01	< 0.01	–
Sb	mg/L	0.04	0.03	–
V	mg/L	< 0.01	< 0.01	–
Zn	mg/L	0.03	0.03	–
DOC	mg/L	16.9	16	–

porewater system define variable water retention capacities. Although local lateral gradients may occur, we expect a relatively homogeneous water flow at unsaturated conditions.

Contrary to dry conditions, a heavy precipitation event leads to formation of distinct water flow zones (Fig. 1, Supplementary Fig. 1), the formation of which is explained with descriptions made in layered soils for instance by Hillel and Baker (1988). Heavy precipitation events result locally in saturated conditions (w_{sat} ~ 34.3 wt.%) in the layers close to the landfill surface (IL, Fig. 1, Supplementary Fig. 1) or in transition zones between disposal sequences. Locally saturated conditions in overlying zones of contrasting hydraulic properties favor the formation of preferential flow zones (PFZ, Fig. 1 and Supplementary Fig. 1). The formation of preferential pathways in coarser grained layers is explained by a narrowing of the flow field due to insufficient runoff from the finer grained layer above. Such effects are likely to be triggered by slight local differences in hydraulic conductivities. The channeling leads to increased vertical flow velocities of the water in these zones. The attainment of saturation of the overlying layer (i.e., infiltration horizon or ponding on compacted layer inside the landfill, Fig. 1) is essential for the formation of a preferential flow system. The relative extent of the preferential flow system is assumed to be directly related to the infiltrating water volume. Capillary effects then lead to (possibly delayed) lateral water transport and thus the formation of an affected zone ($w_{init} < w < w_{sat}$; AUZ, Fig. 1) surrounding the saturated preferential flow zone. The water content of the bottom ash decreases with increasing distance to the preferential flow path. Most of the deposited landfill volume seems to be bypassed (i.e., not directly influenced by heavy precipitation events). Based on our observation during the tracer experiment, we estimated that 70% of the excavated profile area still showed initial disposal conditions (UUZ, Fig. 1, w_{init} = 18.2 wt.%). Preferential flow zones accounted for 5–10% of the cross-section in the coarse-grained part (PFZ; Fig. 1) while the remaining volume (20–25%) consisted of the diffusively formed wet zones (AUZ, Fig. 1) with increased water content. The preferential flow system is present only during heavy precipitation events that result in saturated conditions in any layer in the landfill (e.g., infiltration layer, fine-grained layer, Fig. 1). Due to the saturated conditions and the corresponding high hydraulic conductivity in the PFZ, comparably large vertical water flow velocities are reached in the landfill, explaining the fast reaction of leachate discharge (Q) during heavy precipitation events (Fig. 3).

Interaction of water with bottom ash

Element concentration ranges of landfill leachates are influenced by external factors such as landfill age, bottom ash extraction technique and seasonality (Tables 2 and 3, Supplementary Table 3). However, interaction of water and bottom ash, and thus, leaching of pollutants is mainly controlled by porewater residence time and thus by hydraulic properties of the landfill system. Based on the individual physical and hydraulic properties of each of the defined water reservoirs (i.e., mobile porewater reservoir, immobile porewater reservoir, and preferential flow reservoir), a conceptual estimation of relative residence times, and thus, the degree of interaction between porewater and the deposited solids is elaborated (Fig. 4). It must be noted that this degree of interaction varies very likely as a function of time, especially for the mobile pore reservoir. The variation of the water content results in a variable hydraulic conductivity of the unsaturated medium and thus in a variation of residence times. Rainwater was assumed representing one endmember of the system, while an equilibrated leachate, i.e., porewater saturated with respect to the solid phases in bottom ash, was assumed to represent the other endmember.

Leachate from the preferential flow reservoir was assumed to be far from chemical equilibrium due to the high water flow velocity and consequently to show composition close to the rainwater (Fig. 4). However, it is expected that minimal interaction takes place between the deposited bottom ash and the fast-flowing water. This leads to partial

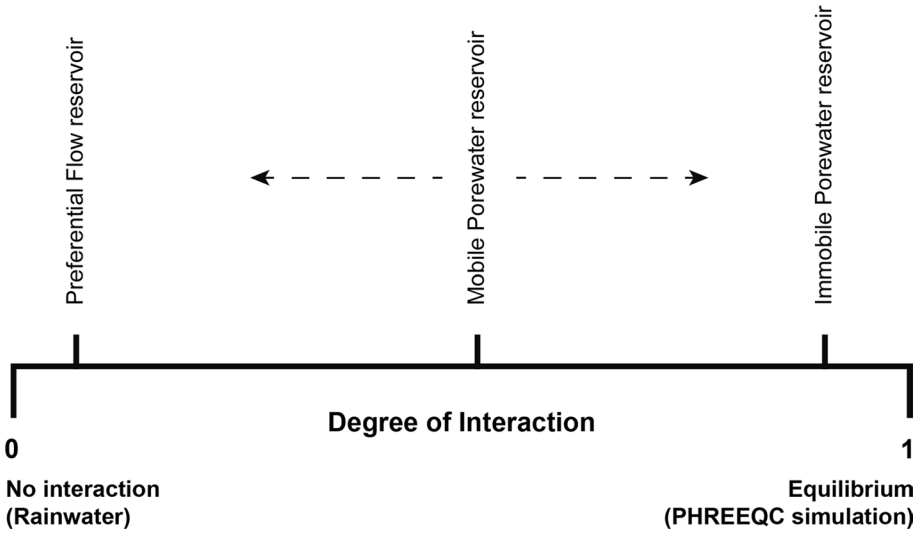

Fig. 4 The degree of interaction of the various water reservoirs with the deposited bottom ash. No interaction is represented by rainwater, while complete interaction (i.e., equilibrium) is demonstrated with the PHREEQC simulation. The dotted arrows indicate the adaptive range of the mobile porewater reservoir due to the variable water content

dissolution and leaching of easily soluble, kinetically unlimited phases (e.g., salts, lime, and anhydrite). Thus, a limited mobilization was assumed.

Solutions from the immobile porewater reservoir are considered as nearly equilibrated with respect to the surrounding bottom ash due to long residence times (nearly no water movement). Johnson et al. (2001) estimated an average residence time for bottom ash landfill leachates of 3 years, which suggests the possibility of a quasi-equilibrated state in such reservoirs. Long interaction times allow complete transformation of lime (CaO) to portlandite ($Ca(OH)_2$). This reaction is assumed to begin as soon as bottom ash interacts with water. While both lime and portlandite are detected in the freshly incinerated bottom ash (i.e., water-free sample IV), none of these phases is observed in the other samples (Supplementary Table 2). In the case of wet extracted bottom ash (e.g., sample I), dissolution of portlandite is expected in the quenching pool. The presence of portlandite in the dry extracted bottom ash sample is explained by the interaction with humid air and the highly reactive bottom ash, since no wetting for transport to the landfill was applied. Similarly, partial dissolution of salts (i.e., halite, sylvite) and anhydrite are expected by contact with water, resulting in lower weight fractions of these phases in wet extracted bottom ashes (Supplementary Table 2). In the context of the immobile porewater system, the complete dissolution of lime/portlandite leads to highly alkaline *pH* conditions in the reservoir, which enhances leaching of metals, silicates, alumosilicates, and oxides (Brady and Walther 1989; Marchioretto et al. 2005; Cappuyns and Swennen 2008). This results in high element concentrations in the porewater and the formation of secondary phases (i.e., ettringite, gypsum, hydrocalumite, and aluminum hydroxide; Eggimann 2008; Glauser 2021). With CO_2 present in the system, formation of carbonates (i.e., calcite, vaterite) is possible. Thermodynamic calculations indicated that immobile porewater is saturated with respect to gibbsite, goethite, and quartz, and is undersaturated with respect to anhydrite, halite, anorthite, calcite, diopside, and magnetite. The formation of carbonates is directly connected to the amount of CO_2 in the system. Assuming rather limited redistribution of CO_2 into the immobile porewater reservoir, the formation of carbonates is considered to play a limited role. The formation of ettringite seems more plausible such a system, although the model indicated undersaturation. The low concentration of Al in the modeled solution is considered as a major issue, which may limit the formation of ettringite. Although no lime or portlandite was detected in the bottom ash of landfill I, their presence would explain the elevated *pH* conditions. However, their consideration in the model would increase the Ca concentration in the system, which was adjusted with the anhydrite content. Reduction of anhydrite would then lead to even lower SO_4 concentrations, which already were underestimated compared to the experimental solutions (Table 4). Further, adjusting halite content to match Cl concentration would lead to an underestimation of Na in the modeled solution compared to the measured concentrations. Consequently, it can be assumed that additional, possibly amorphous phases, have major influence on the *pH* condition and the concentration of Na, Ca, Cl, and SO_4. Their characterization would significantly improve the understanding or the leaching processes of these elements and thus also of the initial weathering of the bottom ash. In case of Al, no primary phase was identified by XRPD (Supplementary Table 2), which may dissolve when interacting with water and thus explain the measured Al concentrations (Table 4). It follows that the measured composition cannot be reproduced by the simulated system. Furthermore, kinetical

limitations and the fact, that the experimental system may not represent a completely equilibrated system, must be considered. Complete dissolution of anhydrite and halite in the immobile porewater systems remains possible.

The interaction degree of the mobile porewater reservoir is mainly controlled by hydraulic properties of the landfill. Due to variation of the landfill water content, and thus, water flow velocity, residence time is assumed to increase during dry conditions. This results in an increased degree of porewater equilibration with solid phases (Fig. 4). During wet seasons, a decrease is expected due to faster water movement. However, dissolution of halite and anhydrite is still considered as primary source of Na, Cl, Ca, and SO_4 concentrations in the leachate samples (Tables 2 and 3). Carbonation processes are considered to contribute most likely during exposure to the atmosphere directly after disposal of bottom ash on the landfill. Thus, it is not expected that this exposure leads to complete cementation of the bottom ash. Therefore, it is assumed that the mobile porewater system in the landfill is regenerated by fresh rainwater, resulting in a constant input of CO_2 into the system. In addition, it is considered that the lime and portlandite dissolution in mobile porewater systems has already progressed in such an extent that these phases are rarely present. Consequently, those dissolution reactions hardly influence the *pH* conditions of the porewater as pH conditions of the leachates show values below *pH* 10. Together with the presence of CO_2 in the mobile porewater, calcite is considered as newly formed Ca-phase. *pH* conditions below *pH* 10 leads to instability of ettringite and thus the release of sulfate into the system (Twidwell and Young 2005; Eggimann 2008; Katsioti et al. 2009). Due to the interconnection of calcite formation and the availability of CO_2-bearing rainwater, transformation of sulfates into carbonates and thus release of SO_4 into the leachate may occur in certain zones of the landfill. Therefore, the location of these zones is associated with the mobile porewater system. Consumption of CO_2 as a function of infiltration depth suggests that this transformation zone propagates downward into the landfill with increasing time. This time dependence may explain the increased sulfate fraction in older landfills (Fig. 2, Supplementary Table 1), while on the cationic side, no trends are observed.

Effects of hydraulic conditions on leachate composition

Considering the water reservoirs and transport pathways found in the landfill (Fig. 1), and their variations in the equilibration degrees (Fig. 4), different scenarios can be considered. These scenarios allow visualization of the landfill discharge during various seasons. The runoff from the different reservoirs is identified as a changing factor, which creates a mixture between the water reservoirs and should correspond to the sampled leachate.

The increasing electrical conductivity during dry seasons is explained by the varying hydraulic conditions in the mobile porewater reservoir. It is assumed that only mobile porewater contribute to the landfill leachate (i.e., preferential flow and immobile porewater reservoir are inactive) and no mixture is taking place. The decrease in water content leads to an increase of the residence time in the mobile porewater system, which increases the degree of interaction (Fig. 4). Consequently, the load and, therefore, the *EC* increase, while the total landfill discharge steadily decreases.

Precipitation events which cause the infiltration layer (IL, Fig. 1) or a ponding system within the landfill (Fig. 1) to reach saturated conditions, result in activation of the preferential flow zone (PFZ, Fig. 1) and therefore the contribution of rainwater via preferential flow path to the landfill leachate. Mixing of the mobile porewater with the preferential flow solution leads to dilution effects, as the latter carries only low elemental loads. As a result, the concentrations of the main elements (Na, Ca, Cl, and SO_4) decrease (Fig. 3). In contrast, the concentrations of selected trace metals (Fe, Al, Cu, and Zn) increase, which is explained by the input of immobile porewater. By activation of the PFZ (Fig. 1), the immobile porewater reservoir in the affected unsaturated zone (AUZ, Fig. 1) is flushed out and mobilized. The concentrations of the major elements are expected to show similar concentrations to those of the mobile porewater, but the significantly longer residence time allows kinetically limited dissolution reactions to occur. Thus, mixing of the immobile porewater shows no effects on the major element concentrations, while the input and thus the total concentration of trace elements in the landfill leachate increases significantly. The behavior of B and Mo follows the trend of major elements, suggesting that dissolution reactions including these elements are not kinetically limited. However, no source phase was identified by XRPD, limiting an exact interpretation of these observations.

Deactivation of the PFZ leads to the reduction of the immobile porewater mobilization until exfiltration is no longer assumed. During the upcoming dry phase directly after a precipitation event, the porewater freshly interacts with the deposited bottom ash. If several precipitation events take place within a short amount of time, a reduced effect on the trace elements is expected, as the interaction time is not long enough, and slow reaction kinetics hinders the dissolution of metal bearing phases. With this temporal influence, different effects can be observed and explain the variation at variable precipitation events. This is shown when comparing the concentration trends of Event 1 and 2, in which Cu, Cr, Sb, and Zn show large differences, while Al, Fe, and V show increasing concentrations and an increase in *pH* is observed in both events (Fig. 3). Besides flushing of the immobile

porewater system, other processes such as desorption and dissolution effects are assumed as possible explanations for heavy metal mobilization during heavy rain events (Johnson et al. 1999).

Conclusions and outlook

With the elaborated data of this study, different water reservoirs and transport pathways in bottom ash landfills are identified: (1) preferential flow path domain (2) mobile porewater domain and (3) immobile porewater reservoir. The landfill leachate is a product of variable volumetric mixing of solutes available in these domains, depending on the hydraulic regime, that is caused by the varying environmental circumstances. Due to high variation in the hydraulic properties of these reservoirs, the individual residence time of the water in the landfill body provides information on the degree of interaction between the water and the bottom ash. This results in a wide spectrum of almost no leaching of the preferential flow water to high leaching of the immobile porewater in the landfill where nearly equilibrated conditions are present.

The elaborated hydraulic properties of a bottom landfill presented in this study serves as a basis for the development of a hydraulic model. To visualize the hydraulic system of the bottom ash landfill during heavy rain events, the conceptual model is currently being implemented with OpenGeoSys (Kolditz et al. 2012). The chemical and mineralogical properties of the porewater systems could be characterized with this study and the concept serves as a basis for the development of a generic hydrogeochemical model. To improve the understanding of the interaction between the leachate and the deposited bottom ash, kinetics and the residence time variations must be considered in future approaches. A coupled implementation of both hydraulic and geochemical aspects in a model will serve as a basis for a better understanding of the landfill system and allows an improved prediction of the evolution of leachate quality.

Supplementary Information The online version contains supplementary material available at https://doi.org/10.1007/s12665-024-11471-y.

Acknowledgements We thank the landfill operators for providing sample materials and information about their treatment and disposal techniques, and for their support during the field experiments. Patrick Kämpfer, Priska Bähler and Philipp Hänggi are thanked for their technical assistance during the different analytical methods concerning chemical analyses of the landfill leachates. Furthermore, we thank Frank Gfeller for his analytical support and instructions during the mineralogical analyses with XRPD and Franziska Nyffenegger for their support during the geotechnical lab experiments.

Author contributions P.I. wrote the main manuscript text and prepared the figures and tables that are included. P.I complied the data presented in the manuscript with the support of G.W. C.W. contributed in data evaluation of chemical experiments and thermodynamic modelling, while T.G. supported the data evaluation of geotechnical and field related experiments and tests. All authors reviewed the manuscript and supported the main author during the writing process.

Funding Open access funding provided by University of Bern The authors have not disclosed any funding. Open access funding was provided by the University of Bern and swissuniversities.

Data availability All additional data are implemented as a Word file (Supplementary Information). Therefore, the data availability for this publication should cover the preferred inclusion in the journal.

Declarations

Competing interests The authors declare no competing interests.

References

Alam Q, Schollbach K, van Hoek C, van der Laan S, de Wolf T, Brouwers HJH (2019) In-depth mineralogical quantification of MSWI bottom ash phases and their association with potentially toxic elements. Waste Manage 87:1–12. https://doi.org/10.1016/j.wasman.2019.01.031

Bayuseno AP, Schmahl WW (2010) Understanding the chemical and mineralogical properties of the inorganic portion of MSWI bottom ash. Waste Manage 30(8–9):1509–1520. https://doi.org/10.1016/j.wasman.2010.03.010

Birgisdóttir H, Pihl KA, Bhander G, Hauschild MZ, Christensen TH (2006) Environmental assessment of roads constructed with and without bottom ash from municipal solid waste incineration. Transp Res Part d 11(5):358–368. https://doi.org/10.1016/j.trd.2006.07.001

Brady, P. V., Walther, J. V. (1989) Controls on silicate dissolution rates in neutral and basic pH solutions at 25°C. Geochimica et Cosmochimica Acta, 53(11), 2823–2830. https://doi.org/10.1016/0016-7037(89)90160-9

Cappuyns V, Swennen R (2008) The application of pH(stat) leaching tests to assess the pH-dependent release of trace metals from soils, sediments and waste materials. J Hazard Mater 158(1):185–195. https://doi.org/10.1016/j.jhazmat.2008.01.058

Chang, E. E., Chiang, P. C., Lu, P. H., Ko, Y. W. (2001) Comparisons of metal leachability for various wastes by extraction and leaching methods. Chemosphere, 45, 91–99. https://doi.org/10.1016/S0045-6535(01)00002-9

Chimenos, J. M., Fernández, A. I., Nadal, R., Espiell, F. (2000) Short-term natural weathering of MSWI bottom ash. Journal of Hazardous Materials, 79(3), 287–299. https://doi.org/10.1016/S0304-3894(00)00270-3

Swiss Confederation (2023a) Gewässerschutzverordnung (GSchV). 1–74. https://www.fedlex.admin.ch/eli/cc/1998/2863_2863_2863/de. Accessed 10 Oct 2023

Swiss Confederation (2023b) Verordnung über die Vermeidung und die Entsorgung von Abfällen (VVEA), 1–50. https://www.fedlex.admin.ch/eli/cc/2015/891/de. Accessed 10 Oct 2023

Dabo D, Badreddine R, De Windt L, Drouadaine I (2009) Ten-year chemical evolution of leachate and municipal solid waste incineration bottom ash used in a test road site. J Hazard Mater 172(2–3):904–913. https://doi.org/10.1016/j.jhazmat.2009.07.083

Ecke H, Sakanakura H, Matsuto T, Tanaka N, Lagerkvist A (2000) State-of-the-art treatment processes for municipal solid waste incineration residues in Japan. Waste Manage Res 18:41–51. https://doi.org/10.1034/j.1399-3070.2000.00097.x

Eggimann, M. (2008) Geochemical Aspects of MSWI Bottom Ash and Implications for Disposal. Dissertation, University of Bern.

Eighmy, T. T., Eusden, J. D., Marsella, K., Hogan, J., Domingo, D., Krzanowski, J. E., Stämpfli, D. (1994) Particle Petrogenesis and Speciation of Elements in MSW incineration Bottom Ashes. In Environmental Aspects of Construction with Waste Materials, Proceeding of the International Conference on Environmental Implications of Construction Materials and Technology Developments (pp. 111–136). https://doi.org/10.1016/s0166-1116(08)71452-3

Engström F, Adolfsson D, Samuelsson C, Sandström Å, Björkman B (2013) A study of the solubility of pure slag minerals. Miner Eng 41:46–52. https://doi.org/10.1016/j.mineng.2012.10.004

Eurostat. (2023). Sustainable development in the European Union. https://ec.europa.eu/eurostat/documents/7870049/16817926/KS-05-23-188-EN-N.pdf/3b2ee0b2-5bc8-d139-ed93-af99827dc50a?version=2.0&t=1688373164670. Accessed 10 Jan 2024

Eusden JD, Eighmy TT, Hockert K, Holland E, Marsella K (1999) Petrogenesis of municipal solid waste combustion bottom ash. Appl Geochem 14(8):1073–1091. https://doi.org/10.1016/s0883-2927(99)00005-0

Federal Office for the Environment (2023) Abfallmengen und Recycling 2022 im Überblick. https://www.bafu.admin.ch/bafu/en/home/topics/waste/state/data.html. Accessed 10 Jan 2024

Glauser, A. (2021) Factors influencing the quality of bottom ash from MSWI in Switzerland. Dissertation, University of Bern.

Hillel, D., Baker, R. S. (1988) A Descriptive Theory Of Fingering During Infitlration Into Layered Soils. Soil Science, 146(1), 51–56. https://journals.lww.com/soilsci/fulltext/1988/07000/a_descriptive_theory_of_fingering_during.8.aspx

Huber F, Blasenbauer D, Aschenbrenner P, Fellner J (2020) Complete determination of the material composition of municipal solid waste incineration bottom ash. Waste Manage 102:677–685. https://doi.org/10.1016/j.wasman.2019.11.036

Johnson, C. A., Richner, G. A., Vitvar, T., Schittli, N., Eberhard, M. (1998) Hydrological and geochemical factors affecting leachate composition in municipal solid waste incinerator bottom ash: Part I: The hydrology of Landfill Lostorf, Switzerland. Journal of Contaminant Hydrology, 33(3–4), 361–376. https://doi.org/10.1016/S0169-7722(98)00077-1

Johnson, C. A., Kaeppeli, M., Brandenberger, S., Ulrich, A., Baumann, W. (1999) Hydrological and geochemical factors affecting leachate composition in municipal solid waste incinerator bottom ash: Part II. The geochemistry of leachate from Landfill Lostorf, Switzerland. J Contaminant Hydrol, 40(3), 239–259. https://doi.org/10.1016/S0169-7722(99)00052-2

Johnson, C. A., Schaap, M. G., Abbaspour, K. C. (2001) Model comparison of flow through a municipal solid waste incinerator ash landfill, . Journal of Hydrology, 243(1–2), 55–72. https://doi.org/10.1016/S0022-1694(00)00404-2

Katsioti M, Mauridou O, Moropoulou A, Aggelakopoulou E, Tsakiridis PE, Agatzini-Leonardou S, Oustadakis P (2009) Utilization of jarosite/alunite residue for mortars restoration production. Mater Struct 43(1–2):167–177. https://doi.org/10.1617/s11527-009-9478-y

Kitamura H, Dahlan AV, Tian Y, Shimaoka T, Yamamoto T, Takahashi F (2019) Intra- and inter-particle heterogeneity of municipal solid waste incineration fly ash particles. J Mater Cycles Waste Manage 21(4):925–941. https://doi.org/10.1007/s10163-019-00853-1

Kolditz O, Bauer S, Bilke L et al (2012) OpenGeoSys: an open-source initiative for numerical simulation of thermo-hydro-mechanical/chemical (THM/C) processes in porous media. Environ Earth Sci 67(2):589–599. https://doi.org/10.1007/s12665-012-1546-x

Marchioretto MM, Bruning H, Rulkens W (2005) Heavy Metals Precipitation in Sewage Sludge. Sep Sci Technol 40(16):3393–3405. https://doi.org/10.1080/01496390500423748

Mehr J, Haupt M, Skutan S, Morf L, Raka Adrianto L, Weibel G, Hellweg S (2021) The environmental performance of enhanced metal recovery from dry municipal solid waste incineration bottom ash. Waste Manage 119:330–341. https://doi.org/10.1016/j.wasman.2020.09.001

Meima, J. A., Comans, R. N. J. (1997) Geochemical modeling of weathering reactions in municipal solid waste incinerator bottom Ash. Environ Sci Technol, 31(5), 1269–1276. https://doi.org/10.1021/es9603158

Federal Office for the Environment (2022) Messmethoden im Abfall- und Altlastenbereich. Federal Office for the Environment. https://www.bafu.admin.ch/bafu/de/home/themen/altlasten/publikationen-studien/publikationen/messmethoden-abfall-altlasten.html. Accessed 10 Oct 2023

Parkhurst, D. L., Appelo, C. A. J. (2013) Description of input and examples for PHREEQC version 3 - A computer program for speciation, batch-reaction, one-dimensional transport, and inverse geochemical calculations. In (pp. 497). US Geological Survey. http://pubs.usgs.gov/tm/06/a43/ Accessed 10 Oct 2023

Piantone P, Bodénan F, Chatelet-Snidaro L (2004) Mineralogical study of secondary mineral phases from weathered MSWI bottom ash: implications for the modelling and trapping of heavy metals. Appl Geochem 19(12):1891–1904. https://doi.org/10.1016/j.apgeochem.2004.05.006

Sabbas T, Polettini A, Pomi R et al (2003) Management of municipal solid waste incineration residues. Waste Manage 23(1):61–88. https://doi.org/10.1016/S0956-053X(02)00161-7

Saffarzadeh A, Shimaoka T, Wei Y, Gardner KH, Musselman CN (2011) Impacts of natural weathering on the transformation/neoformation processes in landfilled MSWI bottom ash: a geoenvironmental perspective. Waste Manage 31(12):2440–2454. https://doi.org/10.1016/j.wasman.2011.07.017

Shimaoka T, Zhang R, Watanabe K (2007) Alterations of municipal solid waste incineration residues in a landfill. Waste Manage 27(10):1444–1451. https://doi.org/10.1016/j.wasman.2007.03.011

Shiota K, Tsujimoto Y, Takaoka M, Oshita K, Fujimori T (2017) Emission of particulate matter from gasification and melting furnace for municipal solid waste in Japan. J Environ Chem Eng 5(2):1703–1710. https://doi.org/10.1016/j.jece.2017.03.010

Spreadbury, C. J., McVay, M., Laux, S. J., Townsend, T. G. (2021) A field-scale evaluation of municipal solid waste incineration bottom ash as a road base material: Considerations for reuse practices. Resources, Conservation and Recycling, 168. https://doi.org/10.1016/j.resconrec.2020.105264

Tanigaki N, Manako K, Osada M (2012) Co-gasification of municipal solid waste and material recovery in a large-scale gasification and melting system. Waste Manage 32(4):667–675. https://doi.org/10.1016/j.wasman.2011.10.019

Twidwell, L., Young, C. (2005). Sulfate Removal Technology Development. EPA Mine Waste Technology program. IAG No. DW89938870–01–1. https://www.researchgate.net/publication/235917765

van der Sloot HA, Kosson DS, Hjelmar O (2001) Characteristics, treatment and utilization of residues from municipal waste incineration. Waste Manage 21:753–765. https://doi.org/10.1016/s0956-053x(01)00009-5